Self-Healing Composite Armor

FINAL REPORT

Scott R. White, Amit Patel
Dept. of Aerospace Engineering
University of Illinois at Urbana-Champaign
205C Talbot Lab
104 S. Wright St.
Urbana, IL 61801
Ph: (217) 333-1077

Contract No. W911NF-06-2-0003

Project Period: 12/8/05-12/07/06

ARL Cooperative Agreement Manager:
Dr. Eric Wetzel
U.S. Army Research Laboratory
ATTN: AMSRD-ARL-WM-MA
2800 Powder Mill Road
Adelphia, MD 20783-1197
Ph: (410) 306-0851

SELF-HEALING COMPOSITES FOR MITIGATION OF IMPACT DAMAGE IN U.S. ARMY APPLICATIONS

A. J. Patel, S. R. White
University of Illinois at Urbana-Champaign, Dept. of Aerospace Engineering
Urbana, IL, 61801

ABSTRACT

In this study, fiber-reinforced composites with self-healing, polymeric matrices are under investigation for mitigation of impact-induced damage. Following the work of White et al. (2001) and Rule et al. (2005), the self-healing properties are engineered into the composite through the inclusion of urea-formaldehyde microcapsules containing dicyclopentadiene (DCPD) liquid healing agent and paraffin wax microspheres containing 10 wt% Grubbs' catalyst. Under low-velocity impact, it is found that self-healing materials are able to repair kissing delaminations, leading to a 51% reduction in damage quantified by a simplified visual technique. Ballistic testing using steel fragment simulating projectiles (FSPs) on composites shows damage modes comparable to the low-rate impact mechanisms. These results suggest that self-healing composites could significantly improve the survivability and sustainability of composite structures in U.S. Army applications.

1. INTRODUCTION

Lightweight armors utilizing polymer matrix composite materials have demonstrated the potential to significantly reduce the weight and increase the mobility and transportability of U.S. Army ground vehicles (Fink, 2000). However, one of the primary limitations of these composite armors is the logistical requirements associated with maintenance and repair. In particular, both low-rate and high-rate impacts induce delaminations that propagate over large regions away from the impact point (Gama et al., 2001). In conventional composites, this damage is typically repaired by removing large areas of composite, or replacing the composite part completely (NASC, 2001; USAF, 2001; Gama et al., 2000; Vaidya et al., 2000). These repair steps are often expensive, time consuming, and require a highly skilled composites technician.

An alternative approach is to utilize self-healing materials (White et al., 2001). In these systems, healing is accomplished by incorporating a microencapsulated healing agent and a catalytic chemical trigger within a polymer matrix. Damage in the form of a crack serves as the triggering mechanism for self-healing, rupturing the embedded microcapsules and releasing healing agent into the crack plane through capillary action. Polymerization of the healing agent is activated by contact with the embedded catalyst, bonding the crack faces (Fig. 1).

Existing studies on the recovery of mechanical properties in self-healing materials have focused on monotonic fracture testing (Brown et al., 2002) and fatigue (Brown et al., 2005). In general, it has been found that the encapsulated monomer approach is very efficient at recovering mechanical integrity, provided that three conditions hold: (1) the cleaved material faces must be in close physical contact, (2) sufficient time must be allowed for completion of the self-healing reactions, and (3) environmental conditions must be amenable to the self-healing chemistry.

The implementation of self-healing materials in armor applications is not straightforward. The damage in the immediate vicinity of the impact point, within a few projectile diameters, often includes significant fiber breakage, matrix cracking, and gross delaminations (McGee and Nemat-Nasser, 2001, DeLuca et al., 1998, Nandlall et al., 1998). Self-healing materials are unlikely to address these damage modes. However, self-healing technologies could be applicable to the broader kissing

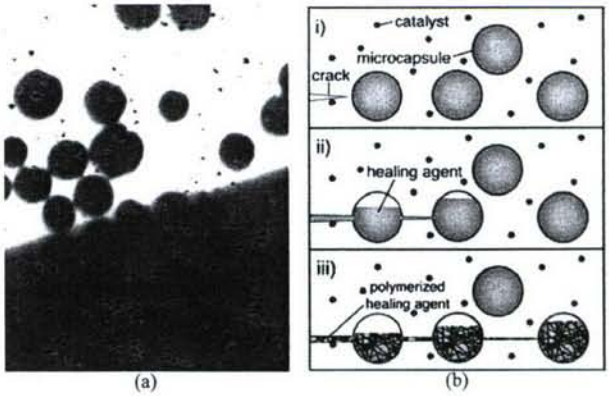

Figure 1: (a) Optical micrograph and (b) schematic demonstrating the self-healing concept. When damage occurs the capsules rupture and release the healing agent into the crack by capillary action. Once exposed to the catalyst the healing agent polymerizes and rebonds the crack plane.

delaminations that typically extend over areas of at least an order of magnitude larger than the projectile frontal area. It is these large areas of delamination that often demand extreme repair steps, or require complete part replacement. Self-healing materials could potentially recover these large kissing delaminations, reducing manual intervention to much simpler and smaller steps in the immediate vicinity of the projectile impact. In this self-healing scenario, repair times, costs, and general logistical burdens would be greatly reduced.

In this study, we explore the applicability of self-healing materials to armor applications. In particular, composites are subject to low-velocity impact, followed by damage visualization and quantification to assess the feasibility of self-healing. These results represent the first attempts to demonstrate self-healing of impact damage. Additional experiments are conducted to examine damage mechanisms in composites subject to ballistic impacts by steel 0.22 caliber (5.59 mm nominal diameter) FSPs, to examine similarities between ballistic and low-speed impact damage modes.

One important consideration when incorporating self-healing materials into a fiber reinforced composite is choosing the correct size scale of the components. Smaller components can reside in narrower interlaminar resin pockets, leading to more even distribution throughout the composite. Although this advantage would motivate the use of very small microcapsules and catalyst microspheres, there are limitations. For microcapsules the amount of healing agent delivered to the crack plane varies linearly with diameter. Thus, at constant microcapsule concentration, an order of magnitude decrease in diameter would correspond to a maximum repairable crack separation reduction of ten times. In addition, wax microspheres will most likely lose their effectiveness to protect the embedded catalyst as size is decreased and surface area to volume correspondingly increases. The above considerations were used in selecting the appropriate size scale of self-healing materials.

2. EXPERIMENTAL

2.1 Materials

2.1.1 Self-healing Components

DCPD filled microcapsules were manufactured by in-situ poly(urea-formaldehyde) microencapsulation (as outlined by Brown et al., 2003) using a Caframo Real Torque Digital™ overhead stirrer with a 63.5 mm Lightnin A-310 impeller blade and a Dataplate Digital Hotplate. Using agitation rate to control microcapsule size, microcapsules of ~35 μm and ~180 μm number average diameter were made using mixer speeds of 1000 rpm and 550 rpm respectively.

Wax-protected catalyst microspheres were made using the same mixer/hotplate setup mentioned above. Using the method described by Rule et al. (2005), paraffin wax microspheres with 10 wt% first generation Grubbs' catalyst were made. It should be noted that 250 mL of 0.2 wt% polyvinyl alcohol aqueous solution was used instead of 225 mL of 0.28 wt% poly(ethylene-co-maleic anhydride) solution. Wax microspheres for control specimens were made by leaving out the catalyst. Microsphere size is also controlled by agitation rate, but plain and catalyst-containing wax microspheres made at the same rpm do not show the same average size. Matching the size distribution between plain and catalyst-loaded wax microspheres proved difficult.

2.1.2 Composite Materials, Lay-up, and Curing

Composite panels for low-velocity impact were approximately 100 × 100 × 4 mm and consisted of 4 plies of 810 g/m^2 5×5 yarns-per-inch plain woven S2 glass fabric (Owens Corning Knytex SBA240F). The initial set of panels consisted of an Epon 828 and diethylene-triamine (DETA) matrix in a 4:1 weight ratio. This non-standard ratio was used to obtain a lower viscosity for the composite lay-up process. Two sets of panels were made to determine the degree of crack reduction due to self-healing. One set of panels (Group SH-I) were made with ~35 μm number average diameter microcapsules and ~270 μm number average diameter wax microspheres containing 10 wt% Grubbs' catalyst. The other set of panels (Group C-I) functioned as controls and were the same except for the use of wax microspheres with no catalyst and with a ~270 μm number average diameter.

Based on the results for these initial panels, another set of panels were manufactured with an Epon 862 and Epi-cure 3274 system in a standard 100:40 weight ratio. The self-healing panels of Group SH-II were made with a 2:1 ratio of ~35 μm to ~180 μm microcapsules, as well as catalyst-containing wax microspheres spun at 1000 rpm. Control panels of Group C-IV were made identical to those of Group SH-II, except they contained plain wax microspheres spun at 600rpm (the motivation for this difference in speed will be discussed in Sec. 3.1). In addition, a set of plain composite panels (Group C-II) and a set of microcapsule-only panels containing 2:1 ratio of ~35 μm to ~180 μm microcapsules (Group C-III) were fabricated as additional controls. Table 1 summarizes the composite panels tested.

Composite fabrication was done using a hand lay-up process in a flat mold between two 6.35 mm thick aluminum plates. A square silicone rubber ring was used as a side wall resin dam, and the top half of the mold consisted of a porous peel ply backed by three layers of bleeder cloth and the top aluminum plate. This setup results in resin bleed-out upwards through the peel ply

Table 1. Summary of materials and testing conditions.

Label	Matrix	Microcapsules	Microspheres	Ceramic	Testing
C-I	Epon 828/DETA	35 μm	270 μm, no catalyst	N	low velocity
SH-I	Epon 828/DETA	35 μm	270 μm, w/catalyst	N	low velocity
C-II	Epon 862/Epi-cure 3274	none	none	N	low velocity
C-III	Epon 862/Epi-cure 3274	35 μm and 180 μm	none	N	low velocity
C-IV	Epon 862/Epi-cure 3274	35 μm and 180 μm	135 μm, no catalyst	N	low velocity
SH-II	Epon 862/Epi-cure 3274	35 μm and 180 μm	135 μm, w/catalyst	N	low velocity
A1-A4	Epon 828/DETA	none	none	N	ballistic
B1-B4	Epon 828/DETA	none	none	Y	ballistic

and into the bleeder cloth during compaction. For Epon 828 and DETA panels, 300 g of epoxy was used, while 400 g was used for the Epon 862 and Epi-cure 3274 panels. Microcapsules and microspheres (33 g and 10 g respectively) were incorporated into composite panels by stirring them into the epoxy prior to lay-up.

Composite panels containing the Epon 828/DETA system were cured at room temperature for 24 hours under compaction, followed by another 24 hours at 35°C with no pressure applied. Panels containing the Epon 862/Epi-cure 3274 system were cured in the same manner, except curing at 35°C was conducted for 48 hours. Panels containing microcapsules (with or without wax microspheres) were compacted in a hot press with about 93 kPa to give a final composite thickness of about 4 mm. To match this thickness, plain composite panels were compacted with about 5 kPa. Using the areal density of the fiberglass fabric and composite thickness, the estimated fiber content of these panels is ~30%.

2.1.3 Ballistic Panels

Two groups of panels were tested ballistically (Table 1). Panels in Group A were simple woven glass-epoxy laminates. Group B consisted of the same woven glass-epoxy laminates, but with small alumina tiles adhesively bonded at the center of their strike faces. The composite panels were approximately 150 × 150 × 3 mm thick, composed of 4 plies of the same S2 glass fabric used in low-velocity impact panels and Epon 828 and DETA (4:1 ratio) epoxy resin. For the Group B specimens, a scrim fabric was used at the ceramic/composite bond line to ensure complete wet-out of the bonded ceramic face. The ceramic tiles for these specimens were CoorsTek AD94 alumina, 48 × 48 × 2 mm thick. The composites were fabricated using a hand lay-up process followed by curing in a hot press. For the Group B specimens, lay-up was done directly on top of the ceramic tiles, integrally bonding them during resin wet-out and cure. The curing conditions for all panels were 93 kPa pressure, with a 24 hour room temperature cure followed by 24 hours at 35°C. The panels interrogated ballistically had no self-healing properties, and were intended as surrogates for future self-healing panels.

Figure 2: Composite panel with 48x48 mm ceramic bonded at center of strike face.

2.2 Testing

2.2.1 Low-Velocity Impact Testing

Impact testing was conducted on an Instron Dynatup 8200 instrumented drop weight impact tester with the sample circularly clamped (76.2 mm diameter) and a spherically shaped impact head of 25.4 mm radius of curvature. Epon 828 and DETA panels were impacted with 13.76 kg from 0.60 m (81 J) on their "rough" side (the top surface that contacted the porous release ply during curing). Epon 862 and Epi-cure 3274 panels were more prone to damage, so impact conditions were reduced to 7.43 kg from 0.60 m (44 J) to prevent excessive damage into the clamped region. In addition, they were impacted on the smoother surface that contacted the bottom of the mold. All impacted self-healing panels were given 48 hours to heal before further testing.

2.2.2 Ballistic Testing

Test panels were securely mounted in a wooden frame. A 12 mm perimeter on the front and back faces of the panels contacted the wooden frame, and this perimeter was lined with two layers of ~1.5-mm-thick rubber on the frame to cushion the panels and ensure a tight fit. Once the panel was in place, the front and back halves of the frame were bolted together. Steel strips were used as reinforcements to prevent damage to the wooden frame. Figures 3 and 4 show the panel support frame. The panels were impacted by 0.22 caliber (5.59 mm nominal diameter) FSPs (DoD, 2006). The projectiles weigh

approximately 1.1 grams each and measure 5.49 mm in diameter. The FSPs were fired from a 0.22 caliber (5.59 mm inside diameter) smooth bore gas gun, using pressurized helium. Velocities were measured using two parallel light-triggered chronographs.

2.2.3 Damage Imaging and Quantification

To image impact damage, tested panels were sectioned through the point of impact into four quarters. The exposed delaminations and matrix cracks were marked by a fluorescent dye penetrant (Zyglo ZL-37) using a technique demonstrated by Kuboki et al. (2002). Images like Figure 5a were obtained that highlight impact damage under UV illumination. For each panel 4 images were obtained, one for each sectioning cut.

The total crack length per imaged edge was used to visually quantify the degree of damage. First, cracks were manually traced over with a pencil tool in Adobe Photoshop CS2. Then, the resulting images were thresholded to yield just the crack tracings, which were in turn skeletonized using a Fovea Pro photo analysis plugin

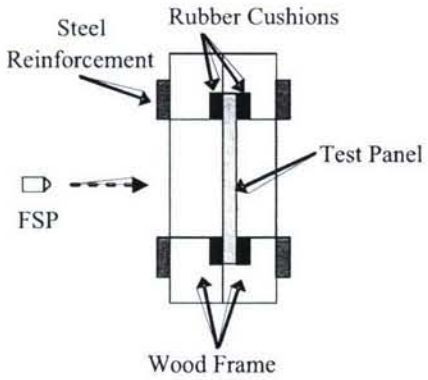

Figure 3: Schematic of panel support frame.

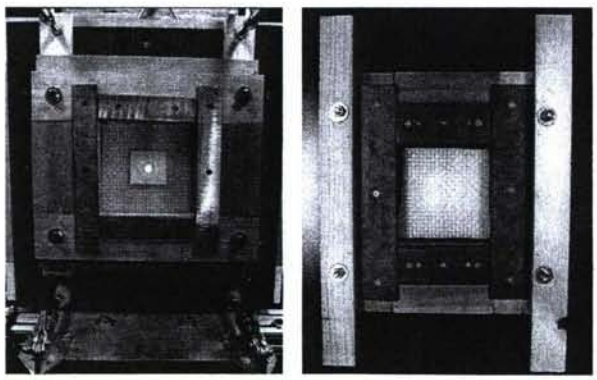

(a) (b)

Figure 4: (a) Front of panel support frame mounted in ballistic test range, panel in place. (b) Back of panel support frame, panel in place.

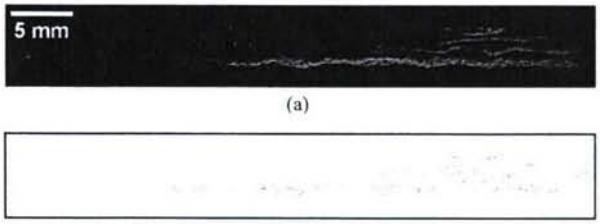

(a)

(b)

Figure 5: (a) Image under UV illumination of fluorescently marked cracks. (b) Skeletonization of marked cracks.

(Fig. 5b). Finally, the total length of the skeleton was then computed using the same plugin software. Thus, a measure of total crack length per image was obtained.

It is important to note that this method of damage quantification reduces the three dimensional damage state to two dimensions. Although this simplification limits the method's accuracy, general trends in the quantity of impact damage can be seen.

3. RESULTS AND DISCUSSION

3.1 Low-velocity Impact Testing

Using the above damage quantification technique, panels from Group SH-I showed a total crack length per imaged edge of 41 ± 14mm, compared to 93 ± 17mm for the full control panels from Group C-I. Closer inspection of the delaminations and cracks by optical and scanning electron microscopy revealed healed regions along the cracks. However, this degree of observed healing did not correspond to the over 50% reduction in total crack length per imaged edge, indicating that the initial state of damage was less in the self-healing panels compared to the full control panels. In addition, further optical and SEM images of delaminated regions cleaved open after healing show only limited patches of healed material localized around wax microspheres (Fig. 6).

A possible cause of the inconsistent degree of damage and the patchy nature of healed material may be poor wax microsphere distribution throughout the composite. The hand lay-up technique employed on Groups SH-I and C-I involved working the resin from the center of the fabric ply out to the edges. This method resulted in wax microspheres being pushed to the edges and an uneven distribution. To combat this problem, subsequent panels (Groups SH-II, C-IV, C-II, and C-III) were fabricated with extra epoxy (400 g versus 300 g) spread evenly initially, thus avoiding the need to work resin to the outside.

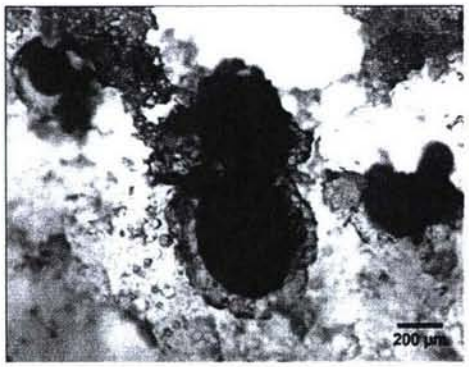

(a)

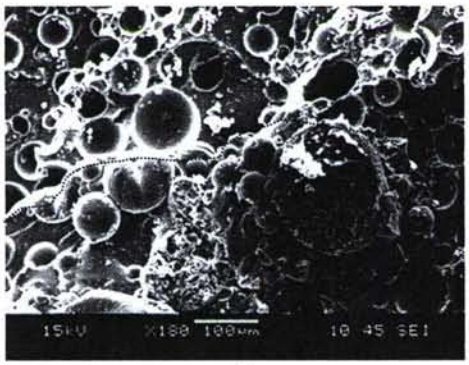

(b)

Fig. 6, (a) Optical image and (b) SEM micrograph of healed patches localized around wax microspheres on cleaved interlaminar region of a panel from Group SH-I.

To further assure consistency in damage patterns, more careful attention was paid to matching wax-protected catalyst microsphere size. Panels from group SH-I and C-I used microspheres matched at a number average diameter of ~270 µm, but as previously noted, plain and catalyst-containing microspheres do not have the same size distribution. For subsequent panels the number density of microspheres in the final composite was matched rather than number average diameter. A simple derivation shows that maintaining the same number density requires matching $\langle d^3 \rangle$, the third moment, instead of $\langle d \rangle$. As a result, 1000 rpm and 600 rpm were chosen as the agitation rates for catalyst-loaded and plain wax microspheres respectively. The smaller size of these microspheres (~135 µm), compared to those of Groups SH-I and C-I, promotes better catalyst distribution.

Further changes were made to enhance self-healing performance. The epoxy resin system was changed from Epon 828 and DETA to Epon 862 and Epi-cure 3274. Catalyst-loaded microspheres appear to tolerate this new system better, as the characteristic browning of deactivated catalyst in Epon 828/DETA specimens was not observed. This system should therefore be advantageous for maintaining catalyst stability as wax microsphere size is reduced. Additionally, the Epon 862 and Epi-cure 3274 system has a longer pot life, making it easier to use in wet lay-up. Furthermore, instead of a single size scale of microcapsules of ~35 µm, a 2:1 ratio of ~35 µm to ~180 µm microcapsules was used to increase the amount of healing agent delivered to the cracks substantially. Finally, panels were impacted on their "smooth" bottom side instead of the "rough" upper surface to avoid deep surface cracks with wide crack separations that were seen in Groups SH-I and C-I. This effect was most likely due to the high concentration of self-healing components on the upper surface caused by the filtration effect of the porous release ply during compaction.

Results for panels of the self–healing Group SH-II show a 51% decrease in total crack length per imaged edge when compared to the corresponding full control system of Group C-IV (Fig. 7). Closer inspection with optical microscopy and SEM (Fig. 8) revealed large tracts of poly-DCPD-filled delaminations with only small unfilled regions, confirming this large reduction in total crack length. In addition, unfilled cracks were predominantly limited to surface cracks and transverse cracks located in regions devoid of self-healing components.

A set of plain composite panels (Group C-II) and microcapsule-only panels (Group C-III) were tested to observe the effects of self-healing components on damage resistance. As seen in Figure 7, there is a negligible increase in total crack length per imaged edge when Group C-III is compared to Group C-II, indicating that the addition of the microcapsules had little effect on impact damage resistance. However, when Group C-IV is compared to Group C-III, a significant jump in total crack length per edge is seen, suggesting that wax microspheres have a detrimental effect on damage resistance. This trend was clearly apparent in some samples in Group C-

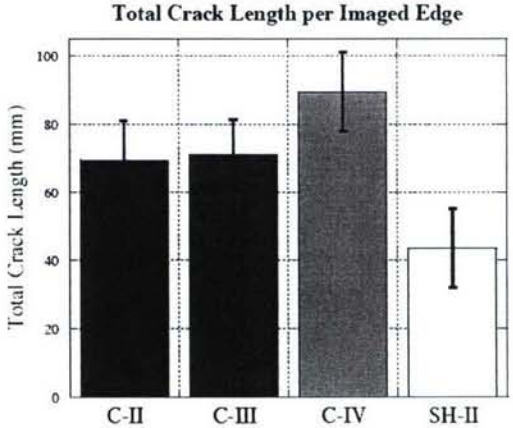

Figure 7: Total crack length per imaged edge for plain (C-II), microcapsule-only (C-III), microcapsule and microsphere (C-IV), and self-healing (SH-II) composite panels. Error bars are ± one standard deviation.

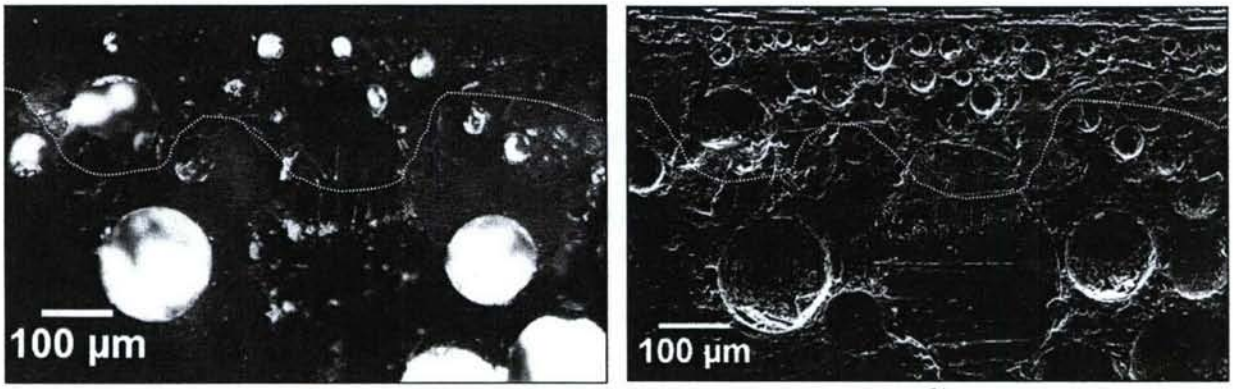

(a) (b)

Figure 8: (a) Optical image and (b) SEM micrograph of a section of rebonded delamination in cross-section from a panel from group SH-II. The dotted lines indicate the path of the delamination across the images. The large circle in the middle is a catalyst-loaded wax microsphere surrounded by smaller microcapsules.

IV that had delaminations that propagated all the way to the clamped edge (Fig. 9). Additionally, self-healing panels of group SH-II show a considerably smaller total crack length per edge than impacted plain composite controls, indicating that self-healing may be able to overcome the decrease in damage resistance imparted by its components.

3.2 Ballistic Testing

Table 2 shows the velocities measured in each of the chronographs for each experiment, as well as the average velocity for each experiment. Data was collected for 4 panels from each group, all shot under similar conditions. The average velocities ranged from 440-471 m/s, with an overall average of 462 m/s.

Figure 10 shows a typical panel from Group A (without ceramic) after ballistic impact, and Figure 11 shows a typical panel from Group B (with ceramic) after ballistic impact. All four Group A panels were penetrated by the projectile. The region in the immediate vicinity of the impact point (within a few mm) had significant local damage, including extensive fiber breakage. Centered around the impact point was a larger region of

Table 2: Average velocities for the eight ballistic experiments.

Panel	Chrony 1 Velocity (m/s)	Chrony 2 Velocity (m/s)	Average Velocity (m/s)
A1	473	467	470
A2	457	450	454
A3	464	457	461
A4	470	463	467
B1	(lost)	440	440
B2	475	467	471
B3	471	464	468
B4	467	462	465
		Min	440
		Max	471
		Average	462

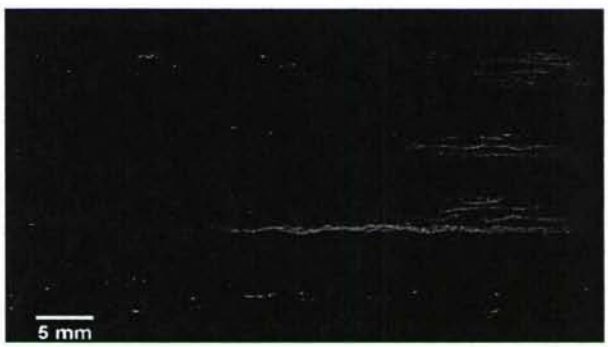

Figure 9: Example images of highlighted damage for (from top to bottom) Groups C-II, C-III, C-IV, and SH-II. The center of impact is the top-right corner of each composite.

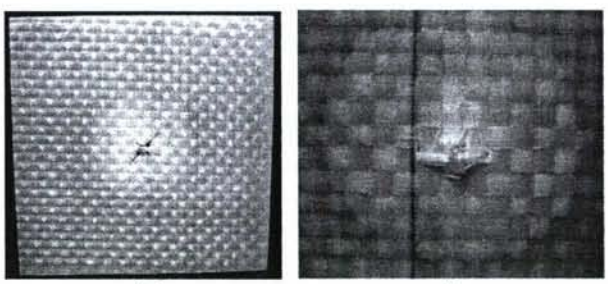

(a) (b)

Figure 10: Damage to composite panel without ceramic tile (Group A) after ballistic impact, front full (a) and rear close-up (b).

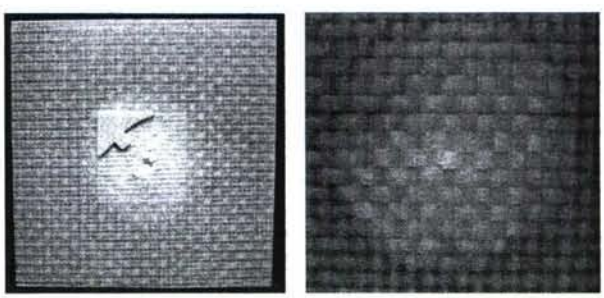

(a) (b)

Figure 11: Damage to composite panel with ceramic tile (Group B) after ballistic impact, front full (a) and rear close-up (b).

delamination, visible as a whitening of the composite. This area was approximately 50-65 mm in diameter. Some permanent deformation of the composite in this region was visible as a slight bowing in the glass-epoxy laminate.

For the Group B specimens, the alumina tile on each panel was completely or almost completely fractured and de-bonded from the glass-epoxy backing after impact. In all cases, the FSP did not penetrate through the glass-epoxy backing, but did create significant localized damage at the impact location. The ballistic impact also created a region of delamination in the glass-epoxy composite approximately 50-75 mm in diameter, similar in size to the delaminations of the Group A specimens. Some permanent bowing of the composite was also evident in Group B specimens. Only one panel in Group B had visible broken fibers in the region of delamination, whereas all of the panels in Group A had broken fibers protruding from the back of the panel where the FSP exited.

Figure 12 shows FSPs before impact, and after impact of unfaced (Group A) and ceramic-faced (Group B) composites. The FSPs that impacted ceramic-faced targets are very deformed, clearly undergoing severe plastic deformation while in contact with the ceramic tile. In contrast, the FSPs that impacted unfaced composite panels show very little or no projectile damage or deformation.

After ballistic impact, samples A1 and B1 were cross sectioned, dye-infused and imaged. The through-the-thickness damage in the ballistically impacted composite panels can be seen in Figure 13. Damage observed in each sample is qualitatively similar to that of the low-velocity drop tower impacted samples (Fig. 9), showing the distinct pattern of interconnecting transverse cracks and delaminations. However, the density of damage appears to be higher in ballistically impacted panels.

Figure 12: 5.59 mm steel FSPs before impact (left), after impacting a ceramic-faced composite (center), and after impacting a composite without a ceramic strike face (right).

CONCLUSIONS AND FUTURE WORK

The conducted study provides visual confirmation of self-healing of low-velocity impact damage to composite materials. A simplified approach to quantifying this damage showed a significant decrease in observed crack length when comparing impacted self-healing panels to impacted control panels. Furthermore, it was observed that the addition of microcapsules to the matrix of the composite had little effect on damage resistance. Incorporation of wax microspheres, on the other hand, increased impact damage considerably. Work is ongoing to identify an alternative catalyst incorporation method with less effect on global mechanical properties.

Although visual confirmation of self-healing was obtained, further work is necessary to test the recovery of mechanical strength. The use of a compression-after-impact (CAI) potentially offers a method to demonstrate mechanical healing. CAI has been an aerospace industry standard for measuring residual strength in impact-damaged composites. Delaminations cause by the impact event lead to local instabilities that lead to localized buckling and the eventual compressive failure of the composite (Zhou and Greaves, 2000). In short, the aim is to use CAI as part of an experimental protocol to obtain quantitative data on the mechanical healing of impact damage in both low-velocity and ballistically impacted panels.

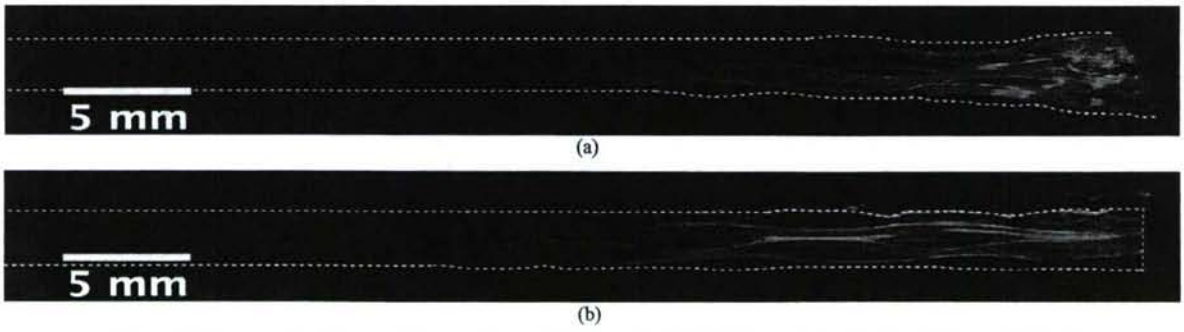

Figure 13: Cross-sectional images of composite panel damage after ballistic impact, (a) unfaced and (b) ceramic-faced.

Although these results are limited in scope, the demonstration of self-healing of composite impact damage has important implications. As the ballistic results show, the modes of damage in ballistically impacted composites are very similar to those of the low-velocity impact. Efforts are underway to demonstrate self-healing directly on ballistically impacted composites. However, the existing observations provide strong evidence that self-healing technologies could be applicable to the repair and recovery of scaled composite armors.

Additional research is also required to address some of the practical limitations of current self-healing systems, such as cost and environmental durability. Furthermore, the experiments in this study allowed 48 hours for completion of self-healing reactions. Although this repair time could be reduced significantly using current chemistries, other studies are underway to identify alternative chemistries that could provide useful self-healing in minutes or seconds.

ACKNOWLEDGEMENTS

The authors would like to acknowledge the assistance of Dick Merrill and Larry Long (ARL) in fixturing and testing of ballistic specimens. The authors would also like to thank John D. Williams and the Materials Testing Instructional Laboratory at the University of Illinois for use of the drop weight impact tester. Other facilities used at the University of Illinois include the Composites Manufacturing Laboratory and Beckman Institute. Electron microscopy was carried out in the Center for Microanalysis of Materials, University of Illinois, which is supported by the US Department of Energy. This project was sponsored by the Army Research Lab.

REFERENCES

Brown, E. N., M. R. Kessler, N. R. Sottos, and S. R. White, 2003: In Situ Poly(urea formaldehyde) Microencapsulation of Dicyclopentadiene. *Journal of Microencapsulation*, **20**, 719-730.

Brown, E. N., N. R. Sottos, S. R. White, 2002: Fracture Testing of a Self-healing Polymer Composite. *Experimental Mechanics*, **42**, 372-379.

Brown, E. N., S. R. White, and N. R. Sottos, 2005: Retardation and Repair of Fatigue Cracks in a Microcapsule Toughened Epoxy Composite- Part I: Manual Infiltration. *Comp. Sci. Tech.*, Special Anniversary Issue, **65**, 2466-2473.

Brown, E. N., S. R. White, and N. R. Sottos, 2005: Retardation and Repair of Fatigue Cracks in a Microcapsule Toughened Epoxy Composite- Part II: In Situ Self-Healing. *Comp. Sci. Tech.*, Special Anniversary Issue, **65**, 2474-2480.

DeLuca, E., J. Prifti, W. Betheny, and S. C. Chou, 1998: Ballistic Impact Damage of S-2 Glass-Reinforced Plastic Structural Armor. *Comp. Sci. Tech.*, **58**, 1453-1461.

Fink, B., 2000: Performance Metrics for Composite Integral Armor. *J. Thermoplastic Comp. Mat.*, **13**, 417-431.

Gama, B. A., T. A. Bogetti, B. K. Fink, C. J. Yu, T. D. Claar, H. H. Eifert, and J. W. Gillespie, Jr., 2001: Aluminum Foam Integral Armor: A New Dimension in Armor Design. *Comp. Struct.*, **52**, 381-395.

Gama, B. A., T. A. Bogetti, B. K. Fink, J. W. Gillespie , Jr., 2000: Processing, Ballistic Testing, and Repair of Composite Integral Armor. *Int. SAMPE Tech. Conf.*, **32**, 802-814.

Kuboki, T., T. Hilvo, and P. Y. B. Jar, 2002: Detection of Interlaminar Cracks in Fiber-reinforced Polymers. *Journal of Materials Science Letters*, **21**, 1789-1791.

McGee, J.D. and S. Nemat-Nasser, 2001: Dynamic Bi-axial Testing of Woven Composites. *Mat. Sci. Eng.*, **A317**, 135–139.

Nandlall, D., K. Williams, and R. Vaziri, 1998: Numerical Simulation of the Ballistic Response of GRP Plates. *Comp. Sci. Tech.*, **58**, 1463-1469.

Naval Air Systems Command (NASC), 2001: Organizational and Intermediate Maintenance, General Composite Repair. Technical Manual NAVAIR 01-1A-2.

Rule, J., Brown, E.N., Sottos, N.R., White, S.R. and Moore, J.S., 2005: Wax-protected Catalyst Microspheres for Efficient Self-healing Materials. *Advanced Materials*, **72**, 205-208.

U.S. Air Force (USAF), 2001: General Advanced Composite Repair Processes Manual. Technical Manual T.O. 1-1-690.

U.S. Department of Defense (DoD), 2006: Detail Specification, Projectile Calibers .22, .30, .50, and 20 mm Fragment-Simulating. MIL-DTL-46593B.

Vaidya, U.K., G. Basappa, B. Mathew, and J. M. Sands, 2000: Flexural Fatigue Response of Repaired S2-Glass/Vinyl Ester Composites. *Int. SAMPE Tech. Conf.*, **32**, 788-801.

White, S. R., N. R. Sottos, P. H. Geubelle, J. S. Moore, M. R. Kessler, S. R. Sriram, E. N. Brown, and S. Viswanathan, 2001: Autonomic Healing of Polymer Composites. *Nature*, **409**, 794-797

Zhou, G. and L.J. Greaves, 2000: Damage Resistance and Tolerance of Thick Laminated Woven Roving GFRP Plates Subjected to Low Velocity Impact. *Impact Behavior of Fibre-Reinforced Composite Materials*, R. Reid and G. Zhou, Eds., Woodhead Publishing Ltd. and CRC Press LLC., 133-185.